NASA/TM–2012-215895

Optical Component Performance for the Ocean Radiometer for Carbon Assessment (ORCA)

Manuel Quijada, Mark Wilson, Timothy Madison, Peter Petrone, and Charles McClain

National Aeronautics and
Space Administration

Goddard Space Flight Center
Greenbelt, Maryland 20771

April 2012

NASA STI Program ... in Profile

Since its founding, NASA has been dedicated to the advancement of aeronautics and space science. The NASA scientific and technical information (STI) program plays a key part in helping NASA maintain this important role.

The NASA STI program operates under the auspices of the Agency Chief Information Officer. It collects, organizes, provides for archiving, and disseminates NASA's STI. The NASA STI program provides access to the NASA Aeronautics and Space Database and its public interface, the NASA Technical Report Server, thus providing one of the largest collections of aeronautical and space science STI in the world. Results are published in both non-NASA channels and by NASA in the NASA STI Report Series, which includes the following report types:

- TECHNICAL PUBLICATION. Reports of completed research or a major significant phase of research that present the results of NASA Programs and include extensive data or theoretical analysis. Includes compilations of significant scientific and technical data and information deemed to be of continuing reference value. NASA counterpart of peer-reviewed formal professional papers but has less stringent limitations on manuscript length and extent of graphic presentations.
- TECHNICAL MEMORANDUM. Scientific and technical findings that are preliminary or of specialized interest, e.g., quick release reports, working papers, and bibliographies that contain minimal annotation. Does not contain extensive analysis.
- CONTRACTOR REPORT. Scientific and technical findings by NASA-sponsored contractors and grantees.
- CONFERENCE PUBLICATION. Collected papers from scientific and technical conferences, symposia, seminars, or other meetings sponsored or co-sponsored by NASA.
- SPECIAL PUBLICATION. Scientific, technical, or historical information from NASA programs, projects, and missions, often concerned with subjects having substantial public interest.
- TECHNICAL TRANSLATION. English-language translations of foreign scientific and technical material pertinent to NASA's mission.

Specialized services also include organizing and publishing research results, distributing specialized research announcements and feeds, providing help desk and personal search support, and enabling data exchange services. For more information about the NASA STI program, see the following:

- Access the NASA STI program home page at http://www.sti.nasa.gov
- E-mail your question via the Internet to help@sti.nasa.gov
- Fax your question to the NASA STI Help Desk at 443-757-5803
- Phone the NASA STI Help Desk at 443-757-5802
- Write to:

  NASA STI Help Desk
  NASA Center for AeroSpace Information
  7115 Standard Drive
  Hanover, MD 21076-1320

Available Only with Approval of Issuing Office (Ocean Ecology Laboratory)
Goddard Space Flight Center, Greenbelt, MD 20771

NASA/TM–2012-215895

Optical Component Performance for the Ocean Radiometer for Carbon Assessment (ORCA)

Manuel Quijada
NASA Goddard Space Flight Center, Greenbelt, MD

Mark Wilson
NASA Goddard Space Flight Center, Greenbelt, MD

Timothy Madison
NASA Goddard Space Flight Center, Greenbelt, MD

Peter Petrone
Sigma Space Corporation, Lanham, MD

Charles McClain
NASA Goddard Space Flight Center, Greenbelt, MD

National Aeronautics and
Space Administration

Goddard Space Flight Center
Greenbelt, Maryland 20771

April 2012

Acknowledgements

The ORCA development activity has been supported under GSFC's Internal Research and Development (IRAD) program and by NASA HQ via the Earth Science Technology Office's Instrument Incubator Program (IIP). The ORCA development team would like to thank those individuals at GSFC and in the ESTO who have been involved in providing this support and for their invaluable guidance.

Do not release on a public Web site.

Level of Review

This material has been technically reviewed by technical management

Abstract

A team at the Goddard Space Flight Center (GSFC) led by Principal Investigator Charles McClain (GSFC; Code 616) has been working on a functional ORCA prototype with flight-like fore and aft optics and scan mechanisms. As part of the development efforts to bring ORCA closer to a flight configuration, we have conducted component-level optical testing and system-level characterizations using non-flight commercial off-the-shelf (COTS) focal plane array detectors. The purpose of this paper is to describe the results of these testings performed at GSFC and the National Institute of Standards and Technology (NIST) at the component and system-level testings respectively.

Contents

Chapter 1

Introduction

The Ocean Radiometer for Carbon Assessment (ORCA) is a new design concept for a next generation ocean color remote sensing satellite. A major goal for this instrument is to accurately measure Top-of-Atmosphere and Surface-Leaving radiance that are used in ocean-color remote sensing to relate the ocean near surface physical and bio-optical properties. The development and testing of the ORCA prototype has been under way at the Goddard Space Flight Center (GSFC) since 2007. ORCA is envisioned as a possible successor to the SeaWiFS instrument.[1] The instrument design reflects "lessons learned" from heritage sensors and is tailored to the new observational requirements recognized for advancing research in ocean biology and biogeochemistry. The purpose of this Technical Memorandum (TM) report is to present piece-part data of components characterization as well as system-level optical performance for this ORCA prototype. Another TM document will discuss a more detailed presentation of ORCA optical design.[2]

The design requirements include a high spectral resolution (up to 5 nm) from UV through visible and short-wave infrared (SWIR) wavelengths (350-2140 nm). There will be a minimum of 26 aggregate bands with a total signal-to-noise (SNR) to exceed 1500 in most UV and visible aggregate bands. Other requirements are: Table 1.1 summarizes the SNR requirements for these 26 aggregate bands in ORCA. These values are partly based on statistics compiled from a SeaWiFS global 1-day L3 data set, presented in table 1.2. The radiance units in this document are those used by MODIS and VIIRS ($W/(m^2 sr \mu m)$). These values can be converted to units used by SeaWiFS ($mW/(cm^2 sr \mu m)$) by dividing them by 10.

The observational requirements listed In Table 1.1 reflect our new understanding of marine systems and their influence on ocean optics. Therefore, these requirements will not be met by any simple expansion of the SeaWiFS or MODIS designs. It is for this reason that these requirements have driven the optical design to include a grating spectrometer. Using diffractive gratings seems an obvious choice in order to simplify the optical design. However, this represents a challenge for an instrument with a polarization sensitivity requirement of less than 1%, given that gratings themselves tend to produce a substantially polarized output beam (as a high as

40%). The proposed solution has been, like in SeaWiFS, to incorporate a depolarizer in order to produce a polarization insensitive optical design.

The purpose of this Technical Memorandum (TM) report is to present characterization of piece-part data for all optical components of the ORCA prototype that is being been built at GSFC since 2008. These component measurements are done in a similar configuration as in the final instrument design (e.g. at the angles of incidence of the final instrument design). By doing this, we are also complying with the requirement that all component characteristics that influence the optical properties of the system shall be measured independently from the component vendor. The equipment used in these component characterizations are state-of-the-art. This is done so that the uncertainties associated with these measurements are also state-of-the-art in order to allow meaningful comparison with system-level performance.

This report is organized in the following fashion. Chapter 2 describes the ORCA optical system. The three following Sections in this Chapter (2.1, 2.2, and 2.3) describe in more details the primary mirrors and the optical performance of the UV-enhanced Ag coating used on this optic. Section 2.4 presents a description of the depolarizer along with some optical performance data. Section 2.7 is dedicated to the slit as well as to a discussion of the Multiwalled Carbon Nanotube coatings used on this component. We will discuss in Chapter 3 spectral performance details for the various components that form part of the spectrograph optics in the blue, red, and Short Wave Infrared (SWIR) channels. In particular, Sec. 3.1 will present optical performance data for the blue- and red-channels dichroics, whereas Sec. 3.2 will describe efficiency measurements on the gratings for each respective channel. Section 3.4 will address the optical performance for the three SWIR bands at 1245, 1640, and 2135 nm. Section 3.3) will concentrate on the performance for the 5 lens assemblies used in the ORCA spectrograph.

The first Sec. 4.1 in Chapter 4 presents total throughput calculation based on piece-part component data for the three main spectrograph channels. The last two sections in this chapter will provide end-to-end system performance in terms of Point Spread Function (PSF) or imaging (Sec. 4.2) and dispersion performance (Sec. 4.3) for the blue and the red-channels of the ORCA prototype.

Table 1.1: Requirements for the ACE mission Ocean Ecology Sensor (OES) center wavelengths λ_{CW}, bandwidth (BW), SNR at Ltyp, typical radiances (Ltyp), and maximum radiances (Lmax) of the nominal 26 multispectral bands. Radiance units are $W/(m^2 \mu m\, sr)$. The SeaWiFS (SeaW) SNR are given for comparison.

Band	λ_{CW} [nm]	BW [nm]	ACE OES SNR (req.)	SNR* (SeaW)	Ltyp	Lmax
1	350	15	300		74.6	356
2	360	15	1000		72.2	376
3	385	15	1000		61.1	381
4	412	15	1000	897	78.6	602
5	425	15	1000		69.5	585
6	443	15	1000	967	70.2	664
7	460	15	1000		68.3	724
8	475	15	1000		61.9	722
9	490	15	1000	1010	53.1	686
10	510	15	1000	1000	45.8	663
11	532	15	1000		39.2	651
12	555	15	1000	870	33.9	643
13	583	15	1000		38.1	624
14	617	15	1000		21.9	582
15	640	10	1000		19.0	564
16	655	15	1000		16.7	535
17	665	10	1000	570	16.0	536
18	678	10	1400		14.5	519
19	710	15	1000		11.9	489
20	748	10	600		9.3	447
21	765	40	600	522	8.3	430
22	820	15	600		5.9	393
23	865	40	600	364	4.5	333
24	1245	20	250		0.88	158
25	1640	40	180		0.29	82
26	2135	50	100		0.08	22

*: SeaWiFS bands have bandwidths of 20 nm for the VIS bands, 40 nm for the NIR bands.

Table 1.2: TOA radiance range encountered in a SeaWiFS global 1-day L3 data set after removing the 0.5% highest and the 0.5% lowest radiances. The values for those bands with no equivalent SeaWiFS band shall be obtained by scaling the ranges of the closest SeaWiFS band by the ratios of the Ltyp from Table 1.1.

SeaWiFS Band number	SeaWiFS Center-wavelength [nm]	L_{low} [W/ ($m^2 \mu m$ sr)]	L_{high} [W/ ($m^2 \mu m$ sr)]
1	412	50	125
2	443	42	101
3	490	32	78
4	510	28	66
5	555	19	52
6	670	10	38
7	765	3.8	19
8	865	2.2	16

Chapter 2

Optical System

The design requirements for ORCA include a high spectral resolution (5 nm) from UV through visible and near-infrared wavelengths. As mentioned earlier, there will be a minimum of 26 bands with a total signal-to-noise (SNR) to exceed 1500 in most UV and visible aggregate bands. There will be a 2-day global coverage at approx. 1.0 Km resolution (noon/sun-synchronous orbit required). Other requirements are:

- Minimum ($< 1\%$) polarization sensitivity (polarization scrambler required),
- Well characterized out-of-band response, minimum electronic cross-talk, and stray light,
- Optimized throughput over the 350-2200 nm bandpass.

The observational requirements listed above reflect our new understanding of marine systems and their influence on ocean optics. Therefore, these requirements will not be met by any simple expansion of the SeaWiFS or MODIS designs. It is for this reason that these requirements have

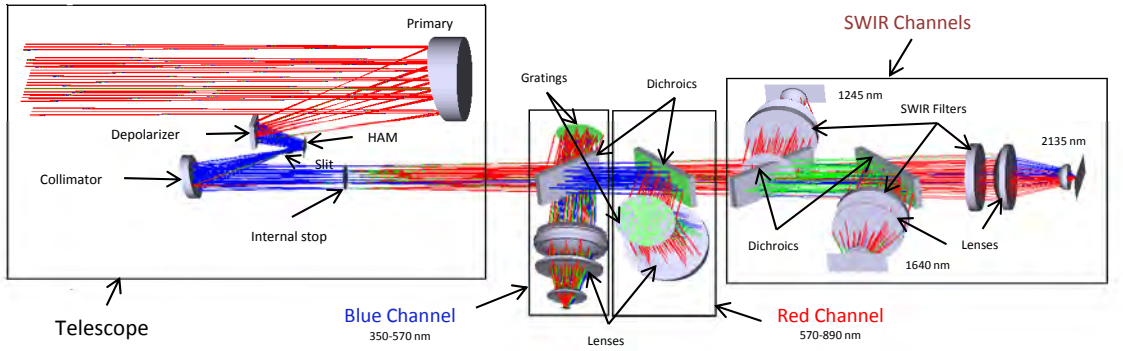

Figure 2.1: Schematic diagram of ORCA optical system.

Table 2.1: Specifications and dimensions (in inches) of the two off-axis ellipsoid (OAE) mirrors.

	SPECIFICATION	**ACTUAL** S/N 001	**ACTUAL** S/N 002
MATERIAL	Zerodur	Zerodur	Zerodur
VERTEX RADIUS	23.6220" ± 0.120"	23.630"	23.630"
CONIC CONSTANT	-0.94659"	-0.947404"	-0.947404"
F1	11.973"	11.975"	sf 11.975"
F2	872.580"	886.58"	886.58"
DIAMETER	3.937" +0.000" /-0.005"	3.936"	3.936"
CLEAR APERTURE	3.543"	sf 3.543"	3.543"
OFF-AXIS DISTANCE	1.969" ± 0.020"	1.970"	1.970"
SCRATCH/DIG	60/40	sf 60/40	60/40
WFE (RMS)	$\lambda/20$	$\lambda/114.9$ @ 633 nm over 99% C.A.	$\lambda/116.2$ @ 633 nm over 99% C.A.
COATING	UV-Enhanced Ag	UV-Enhanced Ag	UV-Enhanced Ag

driven the ORCA optical design to include grating spectrometers. Using diffraction gratings seems an obvious choice in order to simplify the optical design. However, this represents a challenge for an instrument with a polarization sensitivity requirement of less than 1%, given that gratings themselves tend to produce a substantially polarized output beam (as a high as 40%). The proposed solution has been, like in SeaWiFS, to incorporate a depolarizer in order to produce a polarization insensitive optical system. Another paper to be published in these proceedings will described in greater details the design and characterization of this depolarizer.[3]

Figure 2.1 has a layout of the ORCA optical system. The front-end part includes a telescope system with a primary mirror, depolarizer, half-angle mirror (HAM) and slit. After the slit there is a collimator mirror followed by the spectrograph area that is divided in three main sections: a blue channel with spectral coverage from 350 to 570 nm, a red channel that includes a wavelength range from 570 to 890 nm, and a SWIR channel with three discrete bands at 1245, 1640, and 2135 nm. Next sections will describe in more detail the characterization for the telescope optical elements as well as the optical components that form part of the rest of ORCA optical system.

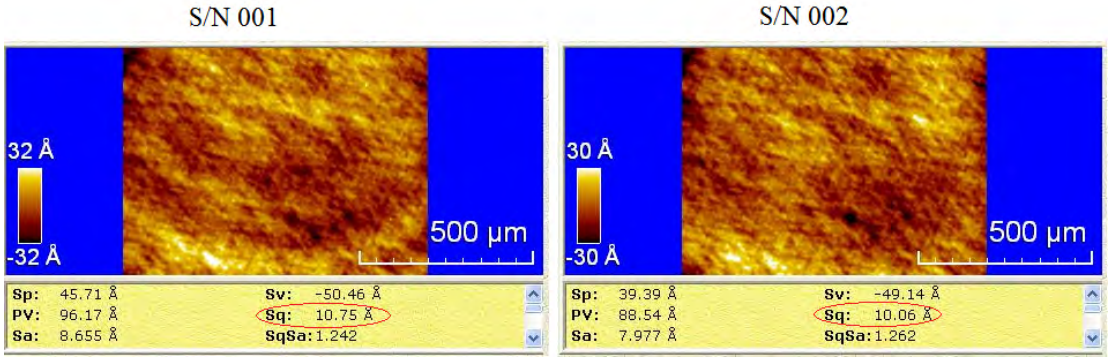

Figure 2.2: Images with results of micro-roughness measurements performed on two mirrors considered for use in the ORCA prototype.

2.1 Telescope Optical Components

The ORCA front-end optical system, a schematic of which is shown on the left side of Fig. 2.1, consists of a telescope with a primary mirror (PM) that collects light from a scene at infinity and refocuses it onto the slit. But before the light reaches the slit, it is intercepted by a polarization scrambler with a reflective coating on the back side, and a double-sided half-angle mirror (HAM), that folds the light on the slit as shown in the figure above. As mentioned earlier, the purpose of this polarization scrambler is to reduce the polarization sensitivity of the ORCA telescope system. It is placed right after the PM in order to prevent any polarization for the scene under observation to propagate through the rest of the system. The scanning mechanism is such that both PM/depolarizer combination and HAM will rotate in synchronization mode around the same axis with HAM rotating at half the speed as that of the PM/depolarizer combination with the speed of the latter set at ~ 6 Hz.

2.2 Primary Mirror

The primary mirror (PM) used in the ORCA telescope is an off-axis ellipsoid (OAE) focusing mirror. The aperture size was determined in order to meet the SNR requirements listed in Table 1.1 for an orbital altitude of 650 km. Even though the focal length was a free parameter in the design, the final number was chosen for a mirror size that would minimize weight in order to reduce inertia for a primary mirror/depolarizer rotating system.

Two versions of this optics were procured and characterizations of these were carried out with the intention of designating the top performer as the "flight" candidate, whereas the second one would be considered as the "spare". Table 2.1 gives a summary of the specifications and the measured performance on these two mirrors identified as S/N 001 and S/N 002 respectively. The results shown in Table 2.1 indicate nearly identical performance between these two, with

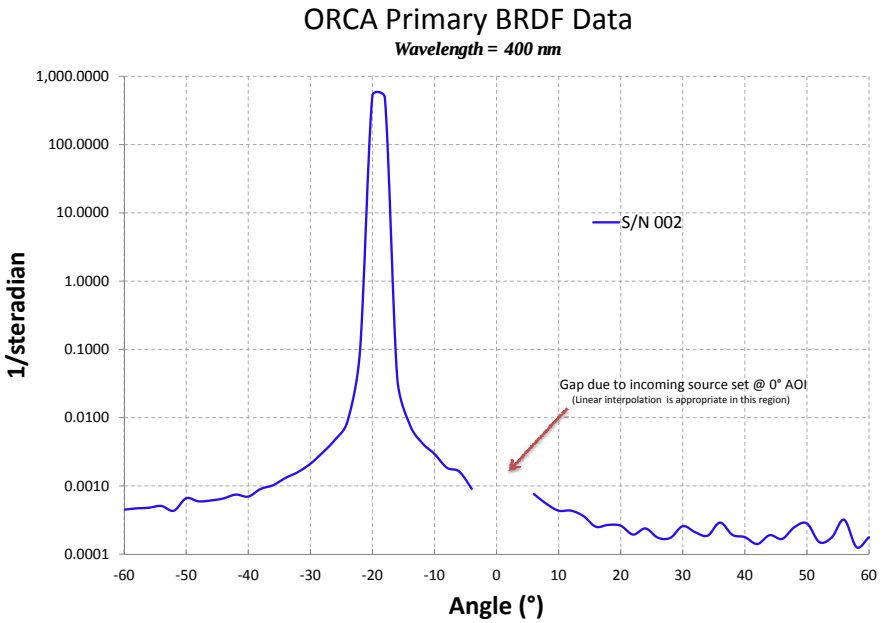

Figure 2.3: Bi-directional reflectance for one of ORCA primary mirrors (S/N 002).

the wavefront error (WFE) being the only exception. This quantity measures the deviation of a wavefront in an optical system from a desired perfect planar wavefront. It also gives an indication of surface accuracy. The results in Table 2.1 showed that the mirror labeled S/N 002 has a smaller WFE at λ 633 nm, and this suggests this mirror has a better optical surface quality.

Figure 2.2 shows results of micro-roughness performed on these two optics using an ADE Phase-Shift (MicroXAM model) surface profiler. Again, we found both of these mirrors showed nearly equal micro-roughness with mirror S/N 002 having a slightly lower microroughness or S_q parameter close to $\sim$ 10.06 $\mathring{A}$ RMS. This compares favorably with results for mirror with S/N 001 of as determined from the results of the S$-q$ parameter equal to $\sim$ 10.75 $\mathring{A}$ RMSin this figure.

We also performed bi-directional reflectance (BDRF) on the mirror labeled S/N 002, which was chosen to be installed in the ORCA prototype. This test was done to further validate the surface quality of this mirror and to asses the directional dependence of scattered light that may influence to the system stray-light performance. As expected from the surface quality results shown in Fig. 2.2, the mirror has a strong specular component that foretell a small scattered light contribution. Indeed, the scattered light component is several orders of magnitude ($\sim 10^{-6}$ to 10^{-7}) smaller than that of the on-axis reflectance.

We will discuss next the performance of the reflecting coating applied to the PM as well as the reflecting components such as the HAM, depolarizers and the collimator mirrors.

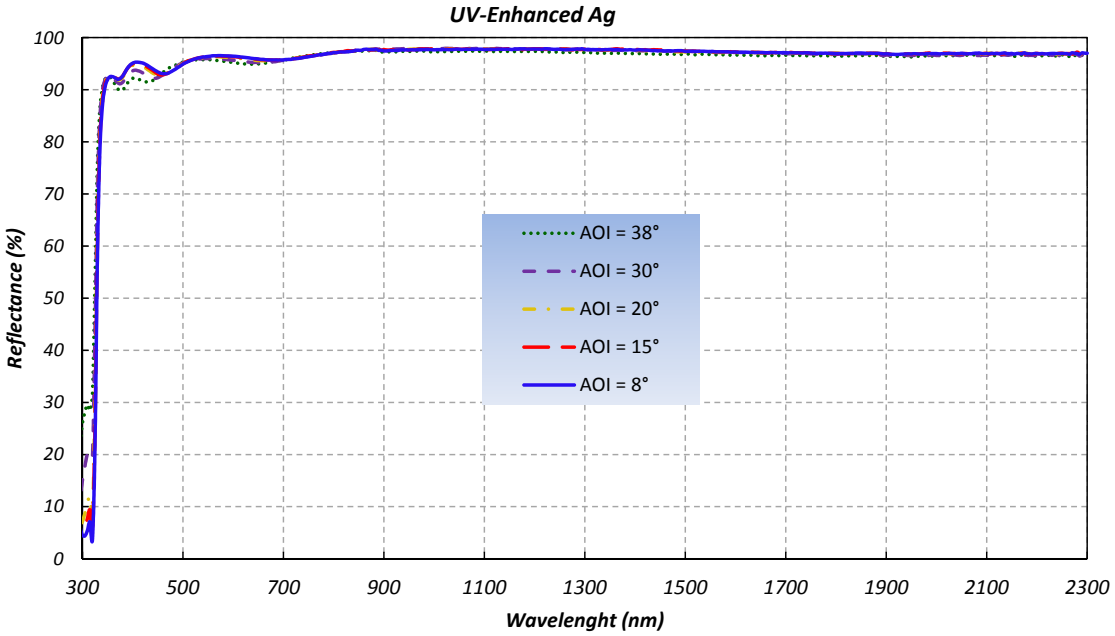

Figure 2.4: Average reflectance of UV-enhanced Ag coating as a function of the angle of incidence.

2.3 UV-Enhanced Ag Coating

Figure 2.4 displays the reflectance performance of the UV-enhanced Ag coating used on the ORCA primary as well as the HAM mirrors. It is a proprietary version of UV-enhanced protected Ag coatings. The reflectance where measured using a Perkin-Elmer 950 (PE950) spectrophotometer fitted with a Universal Reflectance Accessory (URA) that provides absolute reflectance as a function of wavelength (200-3300 nm) and Angle of Incidence (AOI) from 8° to 68°. The reflectance data in Fig. 2.4, taken at various AOI from 8° to 38°, indicate this is a high-throughput coating with an average reflectance of $\sim 98\%$ in the 350 to 2200 nm range. These data also display interference oscillations below 800 nm that are most likely caused by the dielectric overcoats that are used to protect the Ag layer from oxidation and also to boost the reflectance beyond the natural roll-off of Ag that occurs below 400 nm. The reflectance enhancement realized with this coating between 350-400 nm (when compared to bare Ag) was a deciding factor in choosing this coating for ORCA. This choice will ensure the instrument will meet the SNR requirements at the shortest blue-channel band centered at 350 nm.

We also investigated the polarization properties for this coating by measuring reflectance for R_s and R_p polarized light at various AOI from near-normal (8°) to about 38°. This allowed calculation of the diattenuation factor (DF) that is defined by:

$$DF = \frac{R_s - R_p}{R_s + R_p}. \tag{2.1}$$

The results of these calculations are shown in Fig. 2.5 and they indicate a fairly low polarization sensitivity, with the average DF value below 1% for most of the range shown. Only for AOI equal to 38° did the DF exceed the 1% threshold at a wavelength close to 435 nm.

Another consideration is how much variability there is in the coating process from one run to the next. This is important given that there is a requirement that the reflectivity of the HAM mirrors be as similar as possible to avoid stripping in the imagery even though small differences could, in principle, be calibrated out. This is because in scanning mode, ORCA will be using one side of the mirror half the time and the other side will be used the other half. This use imposes a very tight requirement from the instrument calibration point of view that differences in reflectance from one side to the other would be $< 1\%$. Indeed, calculated reflectance differences from side 1 and side 2 of three coated HAM mirrors were less than 1% as shown by the data presented in Sec. 2.6. This indicates this particular UV-enhanced Ag coating process will not be a problem in meeting this requirement.

2.4 Depolarizer

The depolarizer is a commercially available scrambler made by using the principle of the Cornu depolarizer. It consists of two matching wedged pieces of magnesium fluoride (MgF_2) crystals that are glued together so that the optics axis of one is rotated 45° with respect to the other piece.[4] Any ray entering this optics effectively passes through these two wave plates. The thickness of these and therefore their retardance varies across the beam. For this reason, they

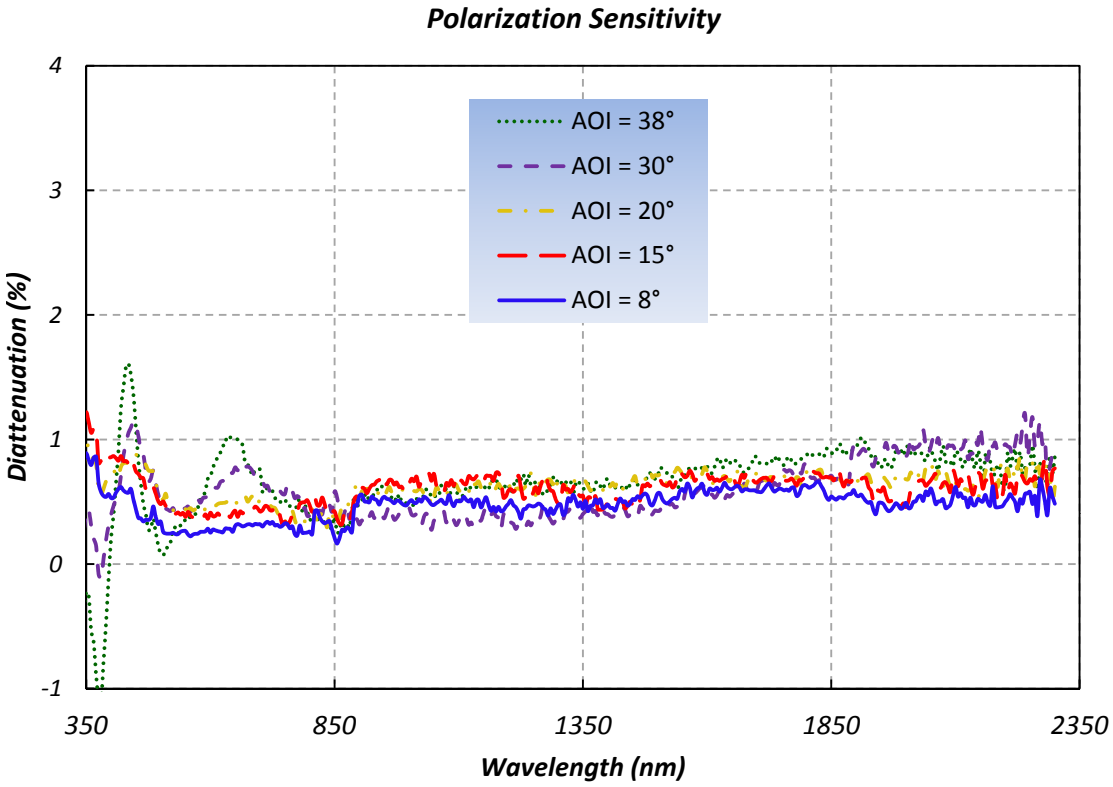

Figure 2.5: Polarization sensitivity of UV-enhanced Ag coatings obtained from Eq. 2.1.

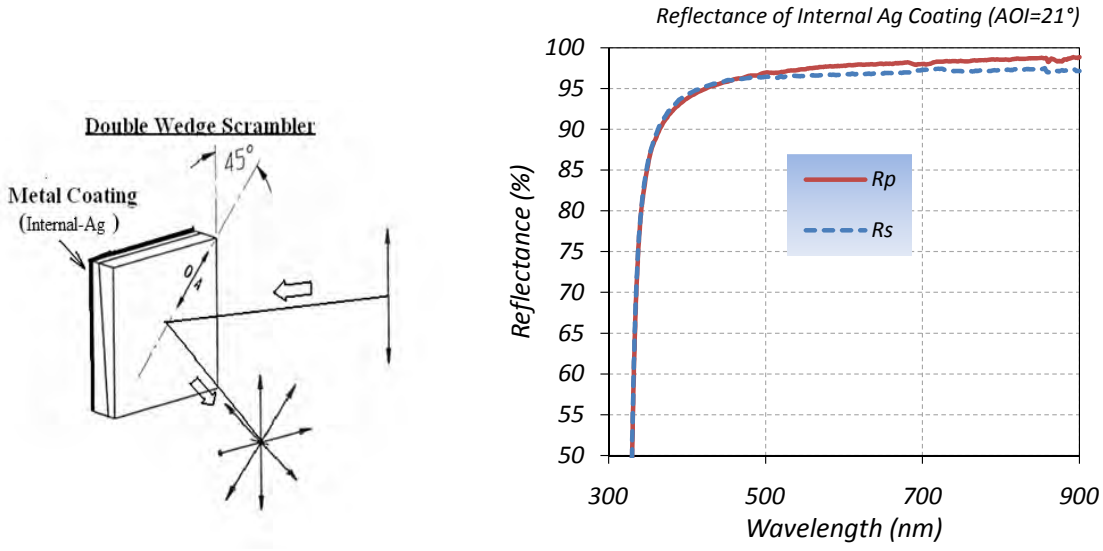

Figure 2.6: Left panel: Polarization scrambler used in reflectance mode made with two wedge pieces of magnesium fluoride. Right panel: Measured polarized reflectance on scrambler at a AOI =21°.

are considered an area depolarizer because at different ray heights on the entrance face of the cube, different thicknesses of left- and right-hand crystals are traversed resulting in an exit polarization angle that is a function of ray height. Thus, the beam will have its polarization state mixed over the beam face. It is also worth mentioning that the phase shift, and hence polarization state mixing are also dependent on wavelength due to dispersion in the glass. The manufacturer of this optic suggests using it in transmission mode where polarized light enters on one side and it emerges unpolarized on the other. However this is not the way in which it will be in the ORCA optical system. As the left panel of Fig. 2.6 shows, we have coated one side of the optics with a reflective coating of protected internal Ag. Hence, the optics is used in a reflection mode (as shown on the left panel of Fig. 2.6), where the depolarizing effect occurs as the beam enters through the non-coated side, goes through the two segmented wedges, then it gets reflected on the coated back and emerges on the same side with an AOI $\simeq 21°$. This is called a double-pass configuration and it is similar to what was used in the SeaWiFS instrument.[1] Additional physical requirements are itemized as follows:

- Clear aperture: 31×31 mm^2
- Full size: 36×36 mm^2
- Center thickness: 5 mm
- Wedge angle in between pieces: 1.5°

- Wedge angle front piece: .55°
- Wavefront error: $\lambda/4$ (at 632 nm)
- Scratch/dig: 60/40

The two items above that reflect surface quality are wavefront error (WFE) and scratch/dig. As mentioned in Sec. 2.2, the WFE parameter measures the distortion of a transmitted or reflected wavefront from a perfect plane wave. It was determined that a value of $\lambda/4$ at a wavelenght of 632 nm would be sufficient to ensure that ORCA will meet its imaging requirement. In regard to the scratch/dig parameter, it was also decided that a nominal value of 60/40 would be adequate. In this case, the "60" digits refer to the maximum width allowance of a surface scratch measured in μm, whereas the "40" digits indicate the maximum diameter allowed for a dig or rough spot in hundredths of a millimeter.

The right side of Fig. 2.6 display the measured reflectance of the scrambler coated on the back side with a proprietary Ag coaying from Quantum Co. The AOI was set in the same configuration as the optic will be used at the nominal value of 21°. The results in this figure show that the average reflectance is around 97%. Although this value is lower than bare Ag over the same wavelength range, it is consistent with the expected losses as light travels through the MgF2 glass.

2.5 Depolarizer Efficiency

Figure 2.7 displays the setup used to measure the depolarizer efficiency. This setup, which is part of a General Purpose Optical Bench (GPOB) accessory, illustrates the beam path after it comes out of the PE950 monochromator. The beam first goes through a linear polarizer which is of the Glan-Taylor calcite prims type. The polarizer can be rotated around its axis to set the linear polarization state of the transmitted or outgoing beam. The beam is next intercepted by the ORCA depolarizer that is configured in reflectance mode as shown in Fig. 2.7. The depolarizer is set to an AOI equal to 20° in order to closely match the angle it will be used in ORCA. After this, the beam is reflected off a fold mirror before it goes through a second polarizer that is denoted as the "Analyzer" in Fig. 2.7. The final beam destination is the integrating sphere that is coupled to the GPOB detector assembly. Depolarizer efficiency data were measured by scanning the PE950 monochromator in the 300-2200 nm spectral range (2 nm resolution) and for various polarizer-analyzer combinations. Figure 2.8 shows data for a regular Al mirror placed in the depolarizer location of Fig. 2.7. These data provide a sanity check on the setup as these results show that when polarizer and analyzer are aligned so that they both transmit the electric field polarization in the same spatial direction, we get a normalized 100% baseline. In addition, the transmitted signal at the detector is nearly zero when polarizer and analyzer are crossed. This corresponds to the the case when the directions of the transmitted electric field polarizations are orthogonal to each other. This figure also shows the absolute polarized reflectance for the same mirror. These data are collected by first removing the analyzer and performing spectra

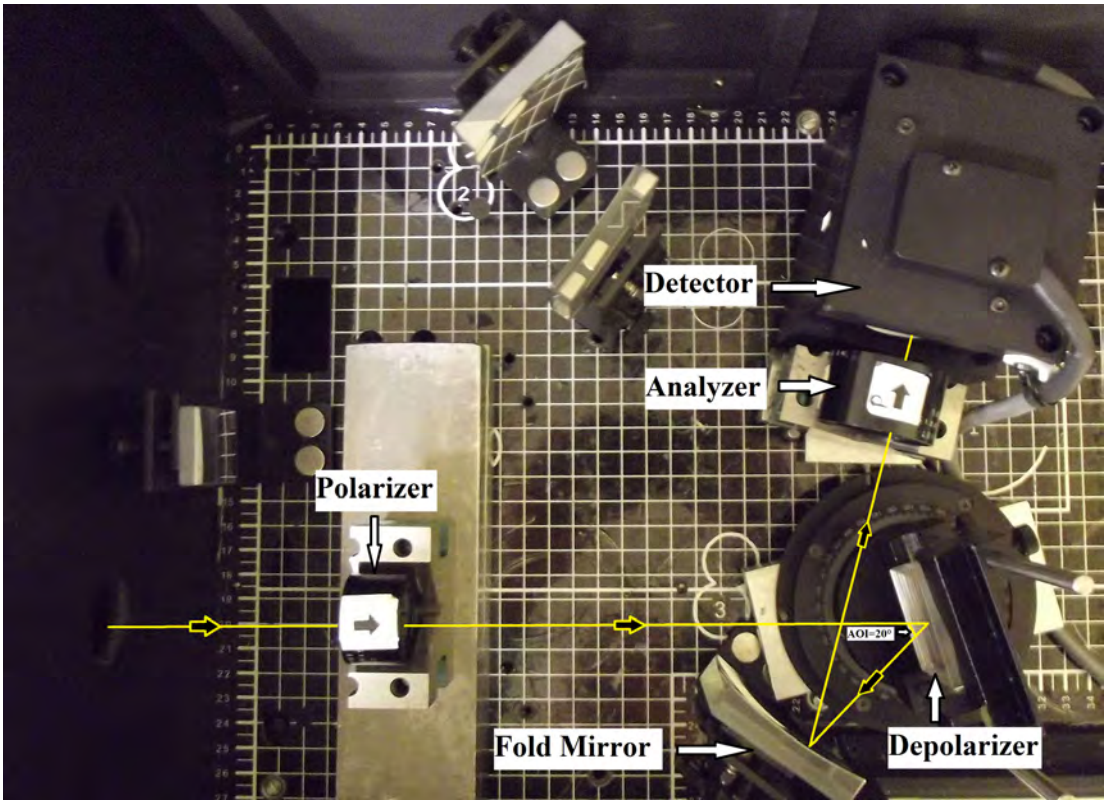

Figure 2.7: Depolarizer efficiency measurement setup.

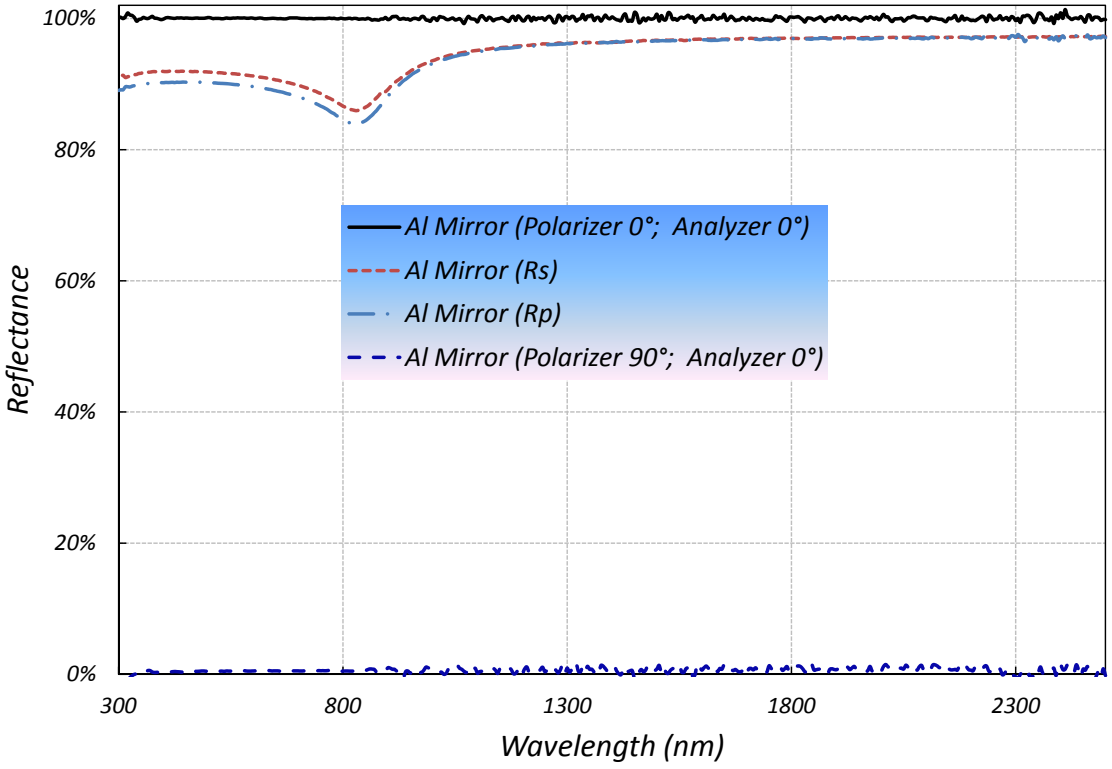

Figure 2.8: Polarized reflectance of an aluminum mirror and spectral scans for polarizer:analyzer orientations co-aligned (0°: 0°) and crossed (90°: 0°).

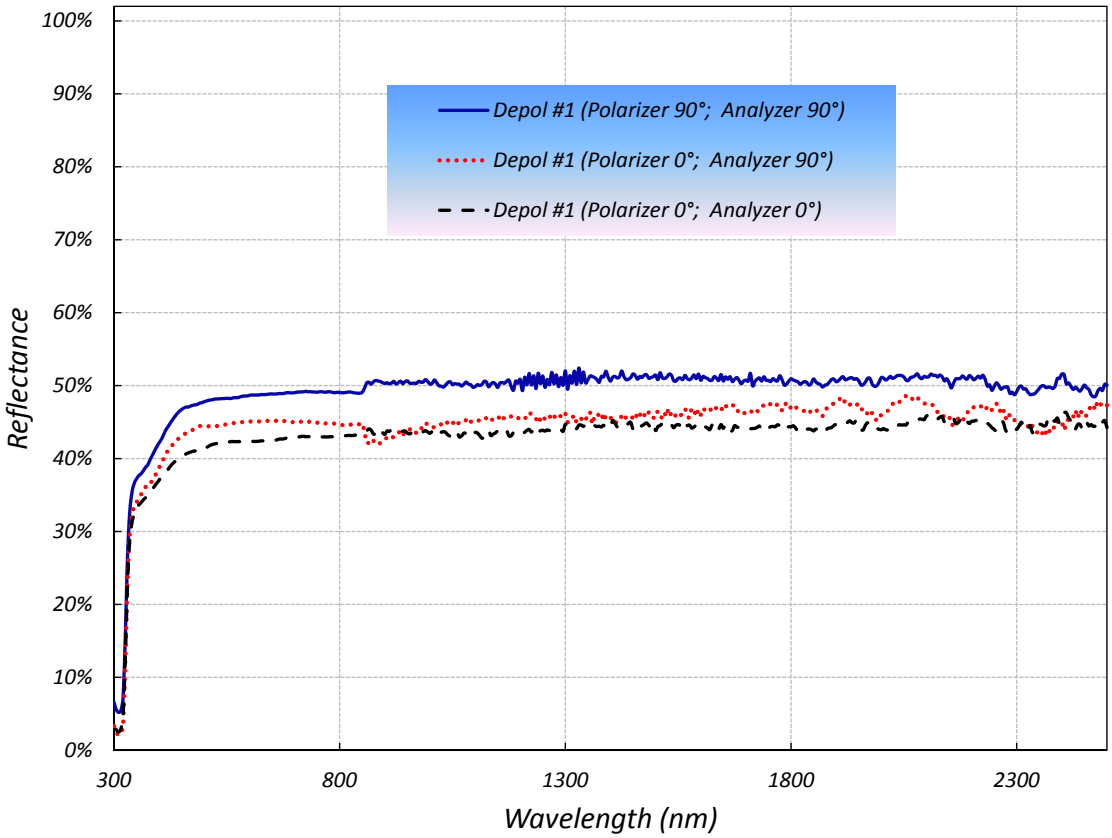

Figure 2.9: Depolarizer efficiency for polarizer-analyzer orientation set at 90°: 90°, 0°: 90°, and 0°: 0°.

scans with polarizer in the vertical or electric field perpendicular to the plane of incidence (R_s) and horizontal or electric field parallel to the plane of incidence (R_p) orientations respectively.

Figure 2.9 displays normalized depolarizer efficiency as a function of wavelength using the configuration shown in Fig. 2.7. The polarizer:analyzer configurations are co-aligned (90°: 90°; 0°: 0°) and crossed (90°: 0°) with all angles measured relative to the depolarizer physical edges. The results indicate the depolarizer is performing as expected; the reflected signal is $\simeq$ 50% of the incoming beam and it is independent of the polarizer:analyzer combinations. This happens as the analyzer only lets through nearly half the signal that is being scrambled by the depolarizer after the beam is linearly polarized by the first depolarizer. Notice also that the level is nearly constant and independent of wavelength indicating the true broadband nature of the depolarizer performance. The slight variance among the three curves shown in Fig 2.9 is the result of a systematic offset in the normalization procedure for these data.

However, the situation is dramatically different when the polarizer:analyzer orientations are

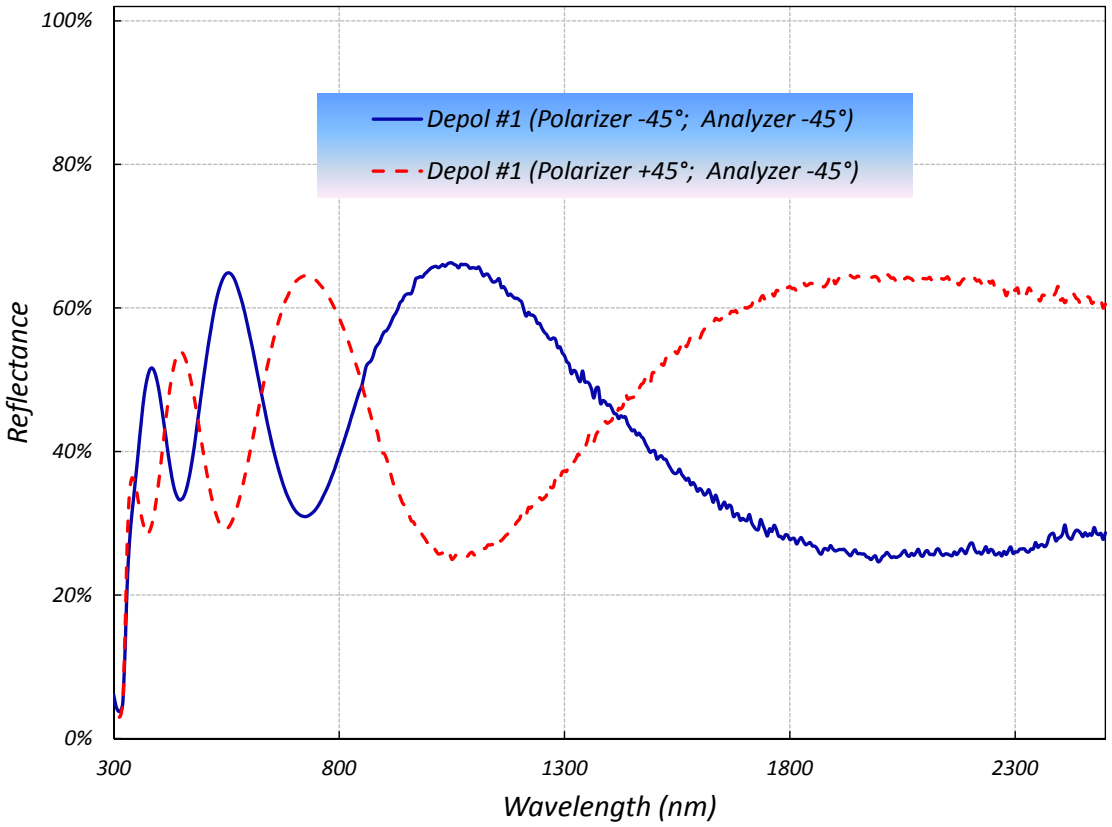

Figure 2.10: Depolarizer efficiency when polarizer-analyzer orientations are co-aligned at $-45°$: $-45°$ or crossed at $+45°$: $-45°$.

Table 2.2: Pre- and post-coat wavefront error data (referenced to HeNe wavelength at 633 nm) for three pre-selected HAM mirror substrates.

Sample S/N	Pre-coat PV	Pre-coat RMS	Pre-coat Power	Post-coat PV	Post-coat RMS	Post-coat Power
# 001; side 1	0.228	0.042	-0.151	0.223	0.039	0.144
# 001; side 2	0.101	0.054	0.187	0.155	0.032	-0.110
# 006; side 1	0.205	0.027	-0.092	0.152	0.025	-0.065
# 006; side 2	0.230	0.040	0.131	0.127	0.029	0.103
# 009; side 1	0.262	0.042	-0.080	0.225	0.048	-0.175
# 009; side 2	0.231	0.037	0.103	0.189	0.039	0.143

halfway between the 0° and 90° angles. To illustrate this, we show in Fig. 2.10 results of depolarizer efficiency with the polarizer:analyzer configurations co-aligned at -45°:-45°) and +45°:−45° (with all angles measured relative to the sample edge). We observe that in this case, the depolarizer efficiency has an oscillatory response that varies between 65% and 25% as a function of wavelength. Furthermore, the phase of these oscillations is dependent upon the exact polarizer:analyzer orientations. These results suggest the depolarizer is only working as a true polarization scrambler at discreet wavelengths when the two curves shown in Fig. 2.10 intersect each other near the 50% points. An important lesson learned during these testing is the fact that the depolarizer will only work in reflectance mode when the correct depolarizer facet or wedge has the mirror coating. The results shown in Fig. 2.9 and Fig. 2.10 correspond to a depolarizer that has the internal Ag coating on the wedge piece with the optic axis along either the 0° or 90° direction relative the part edge. In other words, if the depolarizer is coated on the second wedge or facet that has the optic axis at either ± 45° relative to the first one, the situations shown in Fig. 2.9 and Fig. 2.10 will be completely reversed. These results also offer an important clue to pay close attention to the exact orientation of the depolarizer optical axes relative to those of ORCA in order to minimize the overall instrument polarization sensitivity.

2.6 Half Angle Mirror (HAM)

The half angle mirror (HAM) consists of a flat rectangular piece coated on both sides with the same version of the UV-enhanced Ag coating discussed in Sec. 2.3. Here are the specifications that were used during the procurement process for this optic:

- Clear aperture: 19.9×8.7 mm (based on a 2 mm thick mirror)
- Physical size: 23×12 mm
- Substrate: Fused Silica

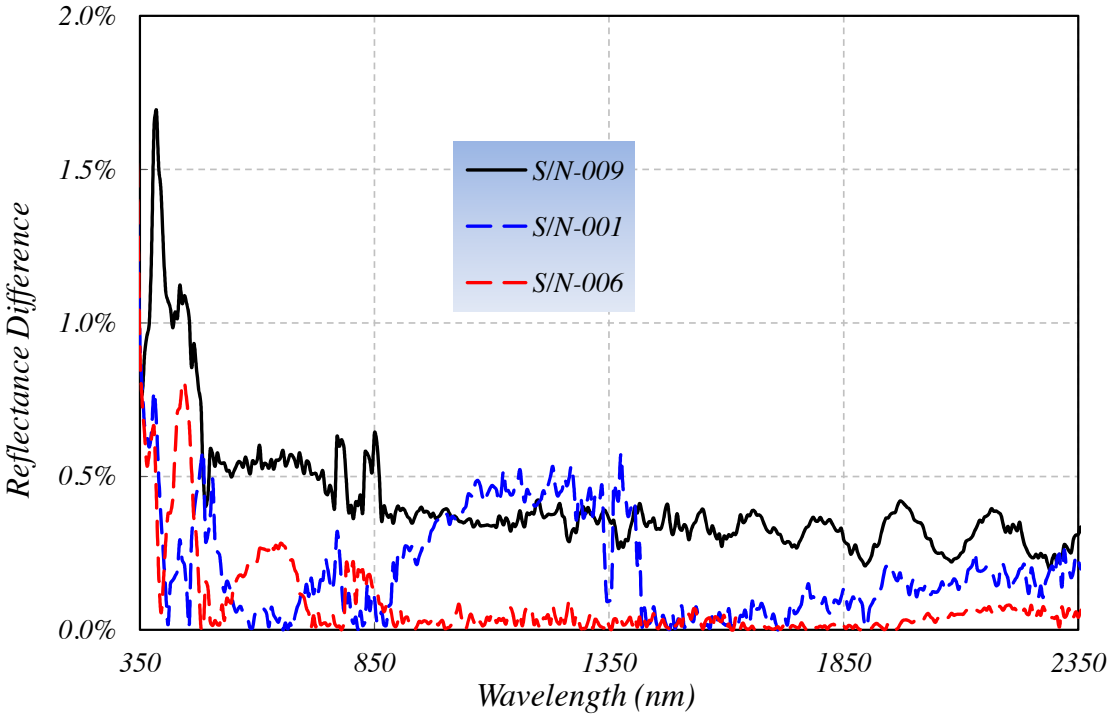

Figure 2.11: Difference in measured reflectance from side 1 and side 2 of the three preselected HAM mirrors after application of the UV-Enhanced Ag mirror.

- Wavefront Error: $\lambda/4$ at 632 nm
- Scratch/dig: 60/40

We obtained a suitable HAM by procuring a total of 10 substrates with the specifications listed above. The three top performers were preselected based on interferometric characterization of their wavefront error at HeNe wavelength (632 nm). Table. 2.2 lists the interferometric data in terms of peak to valley (PV) and RMS flatness for these three pre- and post-coated samples.

A second screening of these mirrors was performed after application of the UV-Enhanced Ag mirror on both sides. Figure 2.11 shows a plot of the difference in the measured reflectance as a function of wavelength for the three preselected mirrors. These results show that the HAM with S/N 009 had the largest peak difference of 1.5 % near 360 nm and average value of 0.4 % across the spectral band shown in Fig. 2.11. The HAM with S/N 006 has the lowest average difference in reflectance ($\sim$ 0.08%) and for this reason it was selected as the HAM installed in the instrument.

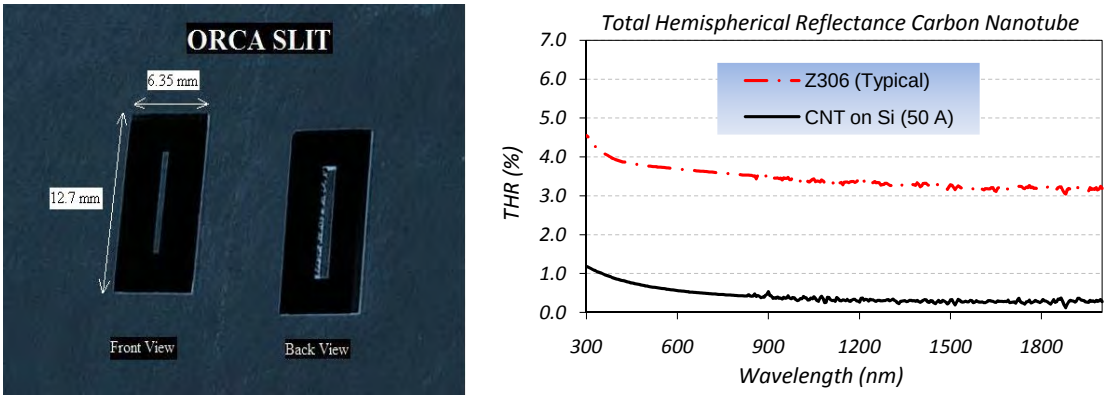

Figure 2.12: Left panel: Front and back slit image with external dimensions. Right panel: Spectral performance of Z306 and carbon nanotube black coatings on Si substrate.

2.7 Slit

The left side of Fig. 2.12 shows images of the slit used in ORCA. The slit is made out of silicon substrate with a flat front and rear surfaces, while the opening in the middle is beveled at 45° on the back side. This is done to remove the possibility of vignetting as the light goes through it. The slit main function is to define the instrument field of view (IFOV) at the detector image plane location. The dimensions of the clear opening are determined through a ray-tracing optical model to ensure that ORCA meets is stated optical performance requirements. For instance, the long dimension ($\sim$ 8.0 mm) is in the along-scan (or spatial) direction and it is related to the instrument requirement of being able to resolve 1.0 Km targets on the ground. Similarly, the narrow ($\sim$ 0.65 mm) opening is along the across-scan (or spectral) direction and it determines the maximum spectral resolution.

Given the fact that the slit is located at the telescope focus point, it is required that it does not become a source of scattered light that may contaminate the signal that goes through. The solution is to have an absorbing coating on the slit substrate to reduce this possibility. To this end, we considered two alternatives: one was a conventional Z306 black pain that has a long heritage in spaceflight application. The second one was a Multi Walled Carbon Nanotube (MWCNT) coating that has been shown to represent the blackest materials known in nature.[5] To further evaluate the suitability of either of the two, the right panel of Fig. 2.12 shows total hemispherical reflectance (THR) measured on representative coatings for each of the two. These results show that indeed, the MWCNT coating has an almost factor of 10 better performance in terms of its ability to absorb light over the wavelength range shown in the figure. These results were a deciding factor in choosing to apply the MWCNT coating on the ORCA slit. Another contributing factor was the fact that silicon is the ideal substrate on which to grow the MWCNT.

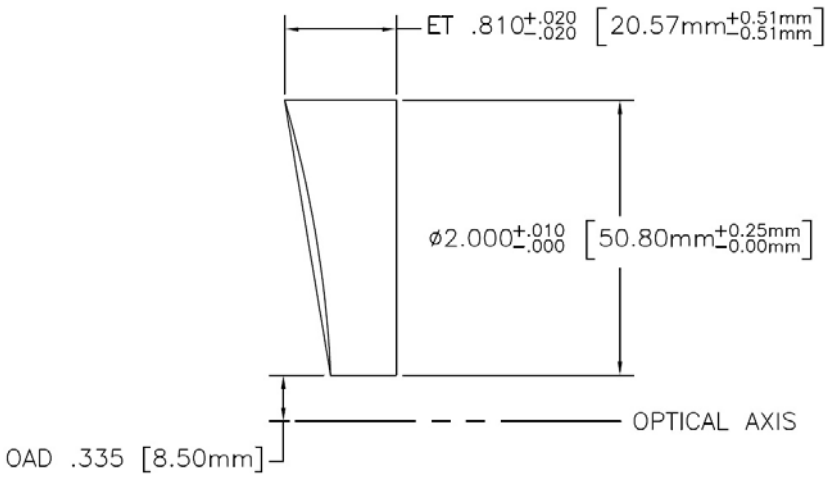

Figure 2.13: Physical dimensions (in inches) for the OAP collimator mirror.

2.8 Collimator

Figure 2.13 shows a diagram with the physical dimensions of the collimator mirror used in ORCA. It is based on an off-axis-parabolic (OAP) mirror provided by NU-TEK Precision Optical Corporation in Aberdeen, MD. The mirror is manufactured from a zerudor glass substrate with a physical diameter of 2" (50.8 mm). The parent focal length is 4" (101.6 mm) with a surface accuracy specified to be $\lambda/10$ at 633 nm. Finally, the reflecting coating on this mirror is a protected Ag mirror proprietary to the NU-TEK company. The reflectance of the coating applied to this mirror is shown in Fig. 2.14. This coating shows a very comparable performance to the one shown in Fig. 2.4 even though they are from different vendors.

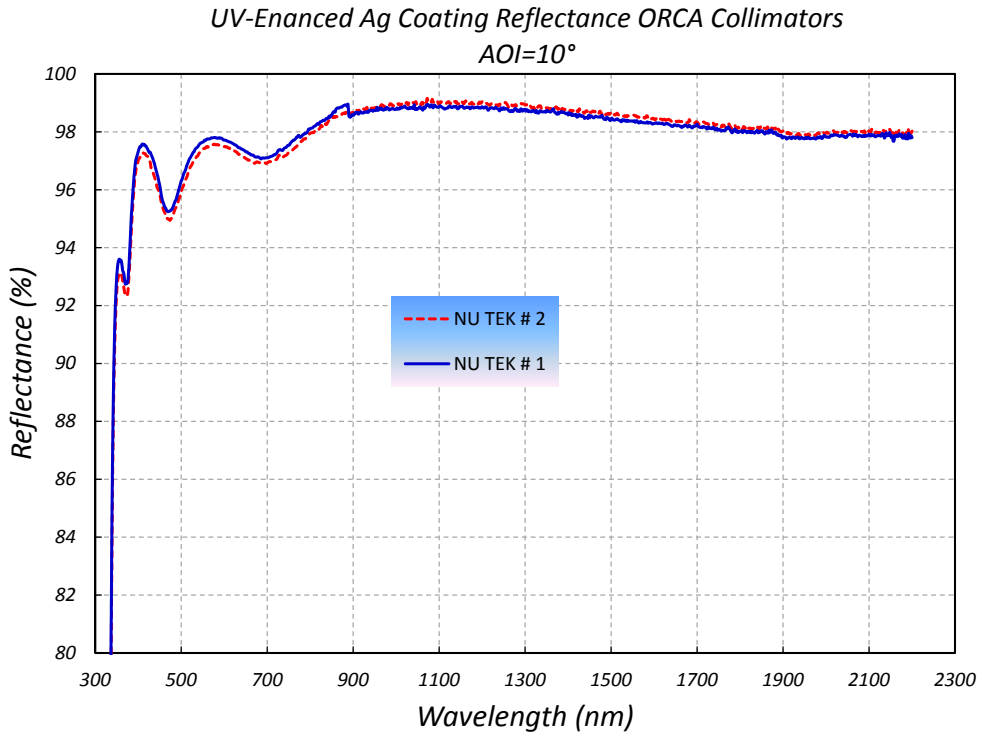

Figure 2.14: Reflectance of UV-enhanced Ag coating applied to the collimator mirror.

Chapter 3

Spectrograph Optics

We now turn our attention at spectral characterization of the optical components that make up the the rest of ORCA optical system. The diagram in Fig. 2.1 shows the arrangement of the various spectrographs with the blue channel being the first after the collimating mirror. The blue channel is followed by the red-channel spectrograph and this is followed by the three SWIR single channels at the back end of the instrument. The following sections are organized according to the sequence in which these optical components appear in the instrument's optical train. Hence, we will discuss first the optical response of the blue- and red-channel dichroic beamsplitters.

3.1 Dichroics

The current design of the ORCA radiometer uses four dichroics in series. They perform a pre-filtering of the radiance from the earth, limiting the range of wavelengths that reach the next optics in each of the five focal planes. In the ORCA application, these dichroics are set at a AOI 45° and they reflect light for wavelengths below a reference wavelength in the dichroics design and they transmit light above this reference wavelength.

In the schematic shown in Fig. 2.1, the first or blue-channel dichroic reflects light in the 350-565 nm range onto the next optics in this channel. This dichoric is designed to transmit light in the 570-2200 nm. This light bundle is next intercepted by a second red-channel dichroic. This second dichroic performs a second splitting of the light, reflecting wavelengths in the 570-890 nm range and transmitting radiance in the 900-2200 nm range. Two more dichroics in the SWIR channel perform more pre-filtering for the three remaining bands in this channel. The SWIR dichroic 1 reflects energy in the 1230 to 1255 nm range. The transmitted light bundle is next separated by the second SWIR dichroic 2 by reflecting radiance in 1600-1650 nm and transmitting light above 1700 nm on to the last SWIR band centered at 2135 nm.

The itemized list below corresponds to the specifications that went out to vendors that were requested to submit quotes;

- Blue dichroic clear aperture: 54.8×30.4 mm (physical size 65×36 mm)
- Blue dichroic average Reflectance: > 95% (Between 345-565 nm)
- Blue dichroic average Transmission > 95% (Between 595-2160 nm)
- Blue dichroic transition width from 5 to 90% (Blue): 20 nm on either side of pass band
- Red dichroic clear aperture: 70.4×31.4 mm (physical size 75×36 mm)
- Red dichroic average Reflectance: > 95% (Between 570-885 nm)
- Red dichroic average Transmission > 95% (Between 905-2160 nm)
- Red dichroic transition width from 5 to 90% (Blue): 20 nm on either side of pass band
- Wavefront Error (front surface): $\lambda/4$ RMS @ 633 nm after coating
- Flatness: < 1/4 wave RMS Transmitted wavefront error at 633 nm over CA (before coating)
- Scratch/dig: 60/40
- Thickness: 8 mm assumed, can be adjusted as needed (6 mm set by vendor)
- Wedge Angle: 0 arcmin.
- Angle of incidence: 45°
- Substrate: Infrared-grade fused silica

As part of the acceptance process, we performed spectral characterization on these optics using the PE950 spectrophotometer. The left panel of Fig. 3.1 gives the spectral response in the form of the s- and p-polarized and average reflectance and average transmittance for the ORCA blue-channel dichroic as a function of wavelength. This figure shows the in-band average reflectance and transmittance are >97% in both cases indicating an excellent performance in this regard. However, the cut-off for the last 90% reflection point for this dichroic falls at 554.9 nm. These data suggest the vendor missed the specified cut-off by about 13 nm. Just as important is the fact that this optic produces a strongly polarized output (∼100%) in the transition region from 550 to 570 nm. This is significant since the last band in the blue channel is centered at 555 nm (with a bandwidth of 15 nm). As it has been reported elsewhere,[3] this caused the instrument to have a polarization sensitivity larger than 1% at this particular band. However, we anticipate that this non-compliance in polarization sensitivity for this band will be resolved by moving the design cut-off upward by at least 15 nm. This may also require a sharpening in the transition width to minimize the possibility of loss in throughput from the next adjacent red-channel band at 583 nm.

The right panel of Fig. 3.1 gives the average reflectance and transmittance for the ORCA red-channel dichroic as a function of wavelength. We find that the in-band average reflectance

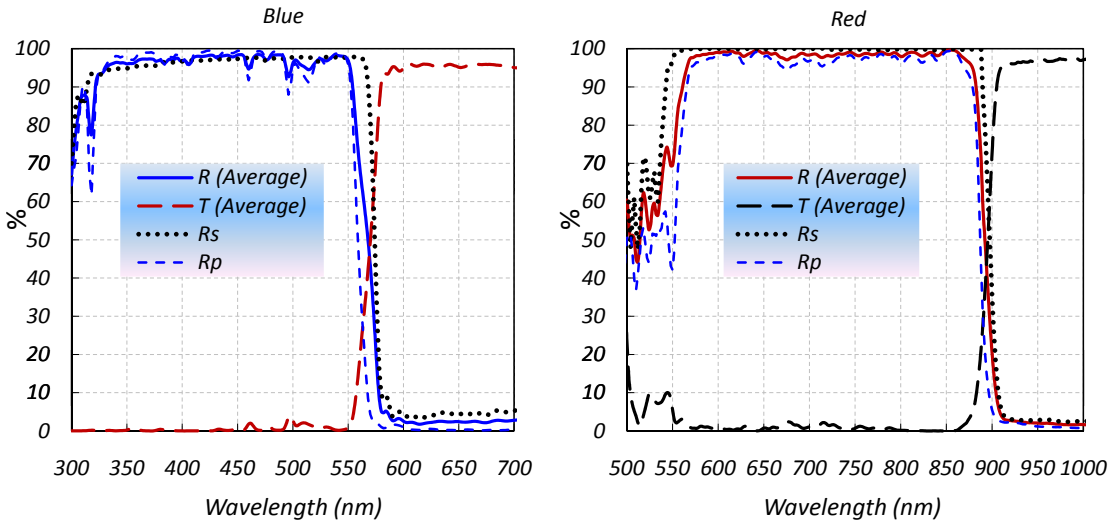

Figure 3.1: Average reflectance and transmittance curves for the blue- (left panel) and red-channel (right panel) dichroics.

and transmittance are 98% in both cases indicating an excellent performance in this regard. Also, the cut-off for the last 90% reflection point for this dichroic falls at 883.5 nm. This is in excellent agreement with the requirement of 885.0 nm.

Table 3.1: List of dichroics along with their corresponding center wavelengths and bandwidth parameters.

Type	λ_0 (nm)	R_{ave} (%)	FWHM (nm)	$\lambda_{on}(90\%)$ (nm)	$\lambda_{off}(90\%)$ (nm)	λ_{on} (1%) (nm)	$\lambda_{off}(1\%)$ (nm)
Blue	437.7	96.8	234.2	< 300.0	554.9	N/A	577.1
Red	721.8	98.3	323.3	< 536.0	883.1	N/A	904.7
SWIR #1	1200.5	98.0	140.8	< 1101	1270.9	N/A	1332.9
SWIR #2	1632.0	94.9	165.9	< 1555	1688.9	1564.4	1749.8

3.2 Gratings

As discussed previously in Sec. 2, the hyper-spectral nature of ORCA along with its high spectral resolution requirements have driven the design to include gratings to provide proper dispersion of the light. This seems an obvious choice given that diffraction gratings are optical components

used to spatially separate polychromatic light (white light) into its constituent optical wavelengths. The simple grating consists of glass substrate with a series of parallel, equally spaced lines on the front surface of the glass. Diffraction gratings are used in such diverse fields as spectroscopy, colorimetry, metrology and laser optics. The next question is to determine the grating parameters, from an optical design model perspective, in order to meet the specifics application needs.

In the case of ORCA, its spectral resolution requirement is such that it will require projection of a monochromatic beam of light to cover an area on the focal plane of roughly 5.0 nm/superpixel, where one superpixel is equal to 8 physical pixels. Hence, it follows that the grating parameters can be determined from the grating equation:

$$d(\sin\,\alpha\ \pm\ \sin\,\beta) = \mathrm{m}\lambda, \tag{3.1}$$

where, α is angle of incidence, β is the angle of diffraction, d is the distance between adjacent grooves, m is the order (integer number) and λ is the wavelength of the incident beam. It is clear from Eq. 3.1 that the condition for the formation of a diffracted order depends on the wavelength of the incident light (λ). Hence, to consider the formation of a spectrum we need to know how the angle of diffraction varies with the incident wavelength. This is found by differentiating Eq. 3.1 with respect to β, assuming the angle of incidence is constant:

$$\frac{\mathrm{d}\beta}{\mathrm{d}\lambda} = \frac{\mathrm{m}}{d\cos\beta}. \tag{3.2}$$

The quantity $\mathrm{d}\beta/\mathrm{d}\lambda$, also known as the angular dispersion, is the change of diffraction angle corresponding to a small change of wavelength. Finally, the linear dispersion of a grating is the product of this term and the effective focal length of the optical system.

Another consideration to take into account in the case of ORCA is the physical size of the slit along the spectral direction (the narrow dimension of the slit image shown in Fig. 2.12). The specifics of how the equations above were used to determine the grating parameters for the ORCA instrument are discussed elsewhere.[2]

In addition to the dispersion requirements given above, the gratings were required to be flat and that conventionally ruled gratings will provide the minimum requirement for average efficiencies across each of the ORCA blue and red channels. Finally, the gratings were used in such a way that the angle of incidence and the angle of the diffracted order were nearly identical ($\alpha \approx \beta$). This is was done to avoid anamorphic distortion of the slit image at the instrument focal plane.

Figure 3.2 shows a schematic of the experimental layout for efficiency measurements of the ORCA gratings usig the GPOB accessory with the PE950 monochromator.

Figure 3.5 has the measured efficiencies for the two gratings used on the ORCA instrument. The left panel of this figure gives the data for the blue channel in the 300-600 nm range, whereas the right panel shows results for the red grating over the 580-880 nm range. Polarized and average efficiencies are plotted as a function of wavelength and these were measured at the appropriate AOI for either grating (28° for the blue and 35° for the red channels). We notice

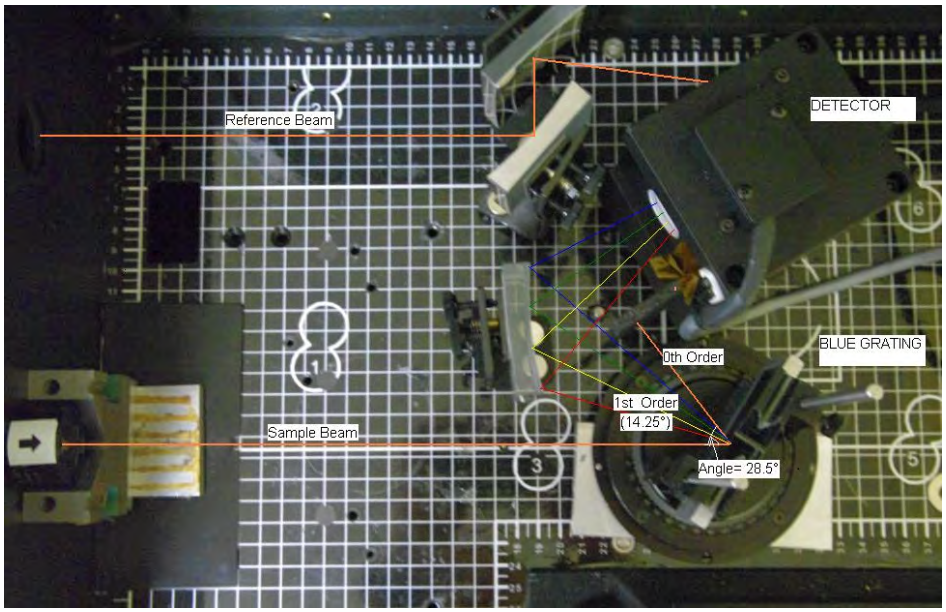

Figure 3.2: Experimental layout for measuring blue-channel grating efficiency.

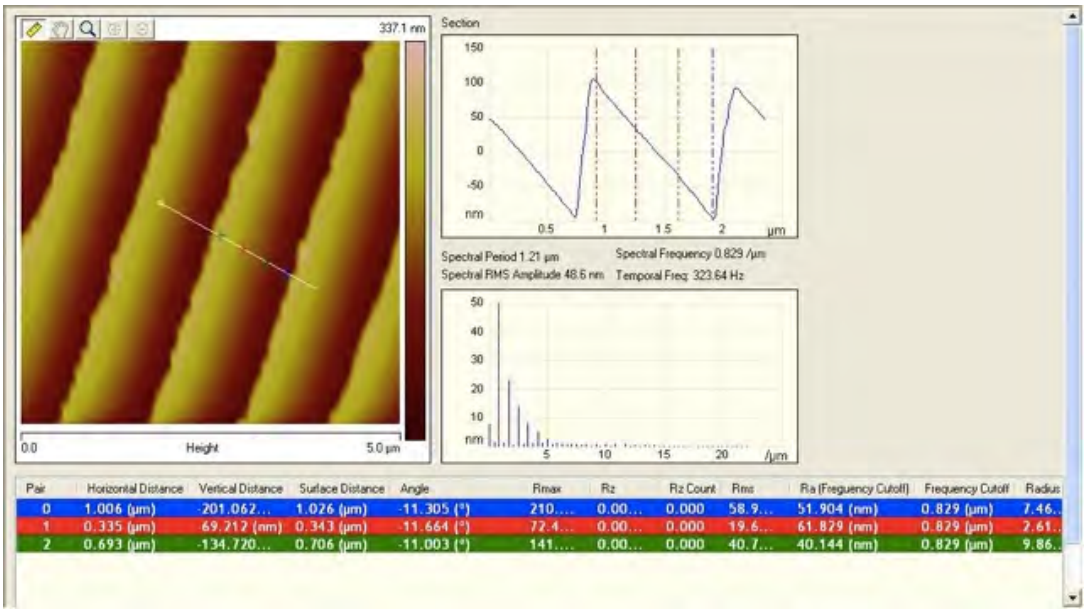

Figure 3.3: Schematic of blue-channel grating groove profile.

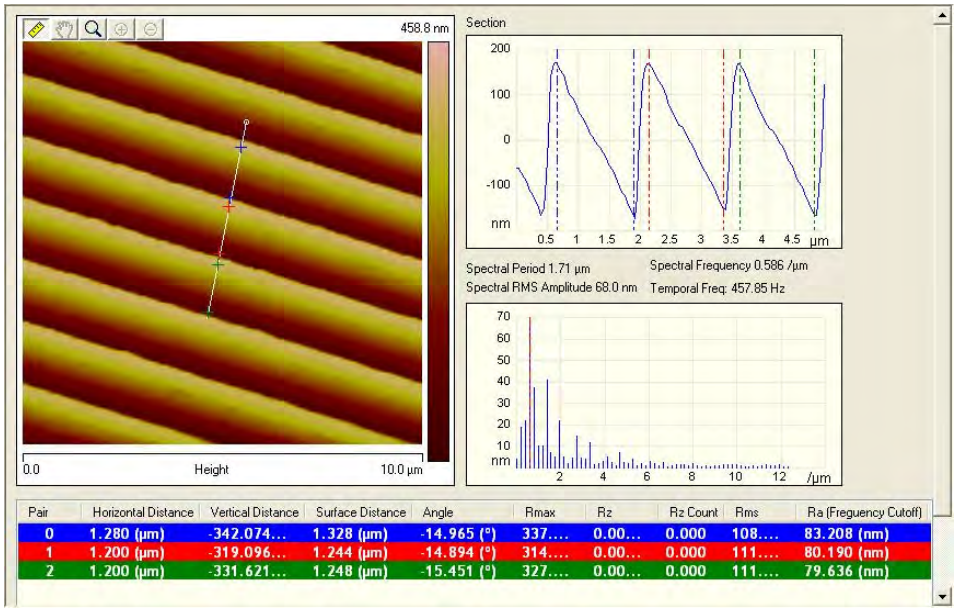

Figure 3.4: Schematic of red-channel grating groove profile.

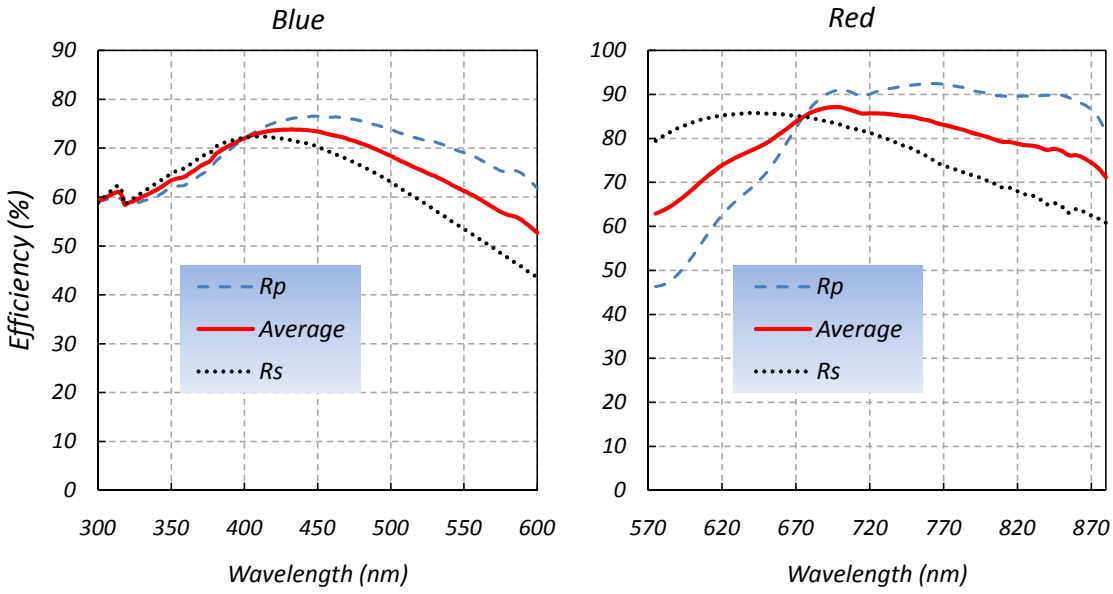

Figure 3.5: Left panel: Polarized and average efficiency results for ORCA blue-channel grating. Right panel: Polarized and average efficiency results for ORCA red-channel grating.

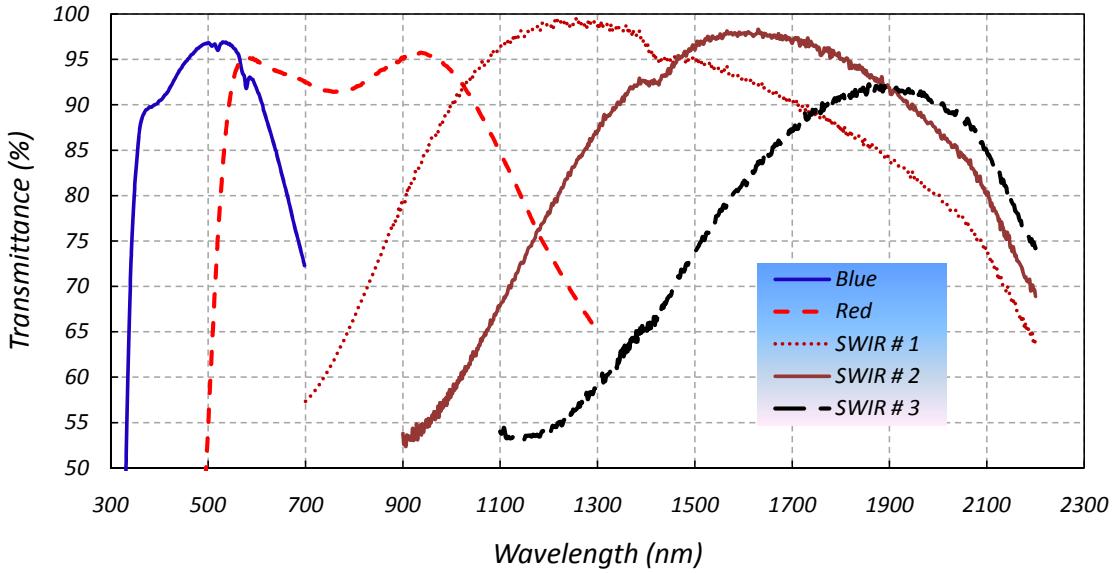

Figure 3.6: Total throughput for each lens assembly in ORCA five channels.

the measured efficiencies are at 60% or higher for both gratings. The maximum polarization sensitivities are <18% for the blue grating, while it is <30% for the red one. A summary of these results are in shown in Table 3.2 where we also show the groove density profile for each of these gratings.

Table 3.2: Measured parameters for blue and red channel gratings.

Channel	Groove Dens.	Order	AOI	Efficiency (Ave.)	Pol. Sen.
Blue	818 lines/mm	1st	28°	66%	$< 18\%$
Red	703 lines/mm	1st	35°	79%	$< 27\%$

3.3 Lenses

The last optical element before the detector focal plane in each of ORCA five channels is the lens assembly. Each of these lenses pick up the collimated (and dispersed output of the gratings in the blue and red channels) and form an image of the light going through the slit on the back of the assembly at best focus where the CCD detectors will be located. The imaging performance requirements are such that these lenses would correct for aberrations of ORCA PM, while producing focused spots at the edges of the slit image (both in spectral and spatial

direction) of 1 physical pixel diameter, with a minimum of slit curvature. The blue-channel lens elements were constructed out of I-line glass materials, whereas standard Schott glass was the material of choice for the red-channel lens elements. The design requirements for both of those two lenses were fully met with all spherical surfaces. The elements in all three SWIR channels were made out of LAK9G15 glass. The throughput in each of the five lenses was maximized by the application of anti-reflection (A/R) coatings to reduce reflection losses. Those A/R coatings were tune to match the respective band-pass for each of the channels.

Figure 3.6 provides the throughput performance in each of the five lenses from measured transmittance as function of wavelength over the full ORCA bandpass range. These results show the A/R coating application was successful in maximizing the transmission in each in-band spectral range. We find that for the blue band, the average in-band transmission is ∼93.5%. Likewise, the red-channel transmission is ∼93.1%. Finally, the corresponding transmission values for the SWIR are 98.9%, 97.7%, and 81.2% for bands 1, 2, and 3 respectively.

Table 3.3: EFL measurements of ORCA five lens assemblies. The last column 4 represents the difference (Δ) between the GFSC and the vendor results.

Lens	GSFC (mm)	Vendor (mm)	Δ (μm)
Blue	48.6	48.50	-808.0
Red	49.0	48.19	-52.0
SWIR 1	43.0	43.30	298.0
SWIR 2	43.2	43.32	168.0
SWIR 3	43.2	43.30	152.0

We also performed effective focal length (EFL) measurements to verify and validate the testing performed by the vendor. Table 3.2

3.4 SWIR Optics

The left panel of Fig. 3.7 gives the average reflectance and transmittance for the two dichroics beamsplitters in SWIR channels. These spectra were collected at the operating angle of incidence of 45°. The first one labeled "BMS-1" splits the beam of light into a reflected component (1130-1270 nm) and a transmitted one (1270-2200 nm). The second dichroic (BMS-2) intercepts the transmitted component from BMS-1 and performs a second split into a reflected (1575-1690 nm) component and a transmitted one (1690-2200 nm). The right side of Fig. 3.7 displays the transmission bandwidth shape for each of the three SWIR dichroic filters. These are the optics that define the actual bandpass for each of the three SWIR bands at 1245, 1640, and 2135 nm. They are placed in front of the respective lenses that re-image the collimated beam on the back on the corresponding focal plane detectors. The filter responses give the principal definition of

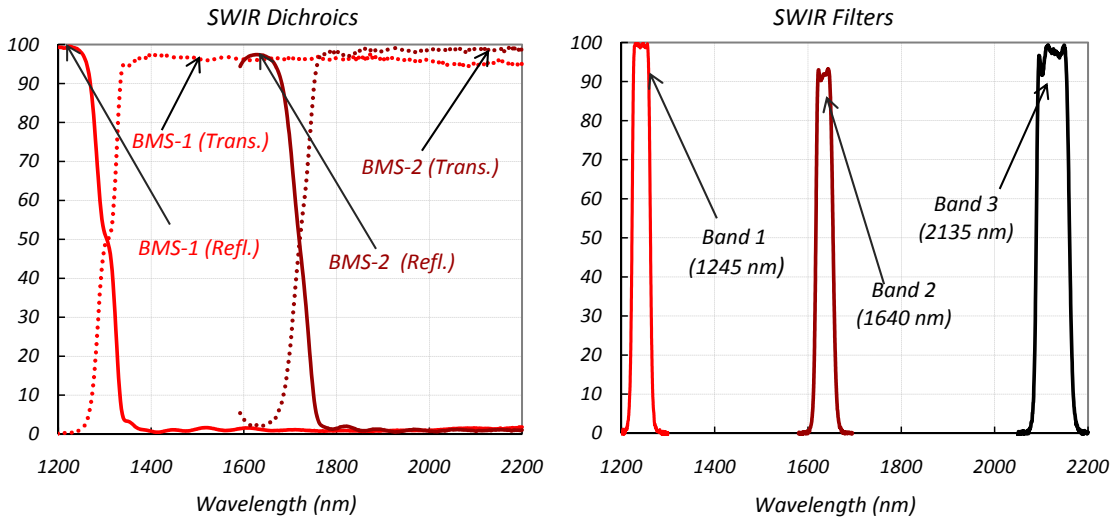

Figure 3.7: Left panel: Reflectance and transmittance for SWIR beamsplitters 1 and 2. Right panel: Transmittance for the band-pass filters for the three SWIR bands.

the SWIR bands in terms of: throughput from the average transmission , the center wavelength; the band edges from the full-width-half-maximum, and the extended band edges from the 1% points.

Table 3.4: List of the three SWIR narrow band-pass filters, along with their corresponding center wavelengths and bandwidth parameters.

Filter #	λ_0 (nm)	T_{ave} (%)	FWHM (nm)	λ_{on} (50%) (nm)	λ_{off} (50%) (nm)	λ_{on} (1%) (nm)	λ_{off} (1%) (nm)
1	1242.2	98.7	39.9	1222.5	1262.4	1218.0	1267.4
2	1634.0	91.1	38.0	1616.4	1654.4	1611.7	1661.3
3	2134.0	96.6	72.0	2089.3	2161.2	2084.0	2169.0

Tables 3.1 and 3.4 give a summary for all the dichroic and filter parameters derived from data shown in Figures 3.1 and 3.7. We observe that with the exception of the blue-channel dichroic that missed the long-side reflectance λ_{off} by 13 nm, the other optical components show excellent performance and they will ensure that ORCA will meet its spectral performance requirements.

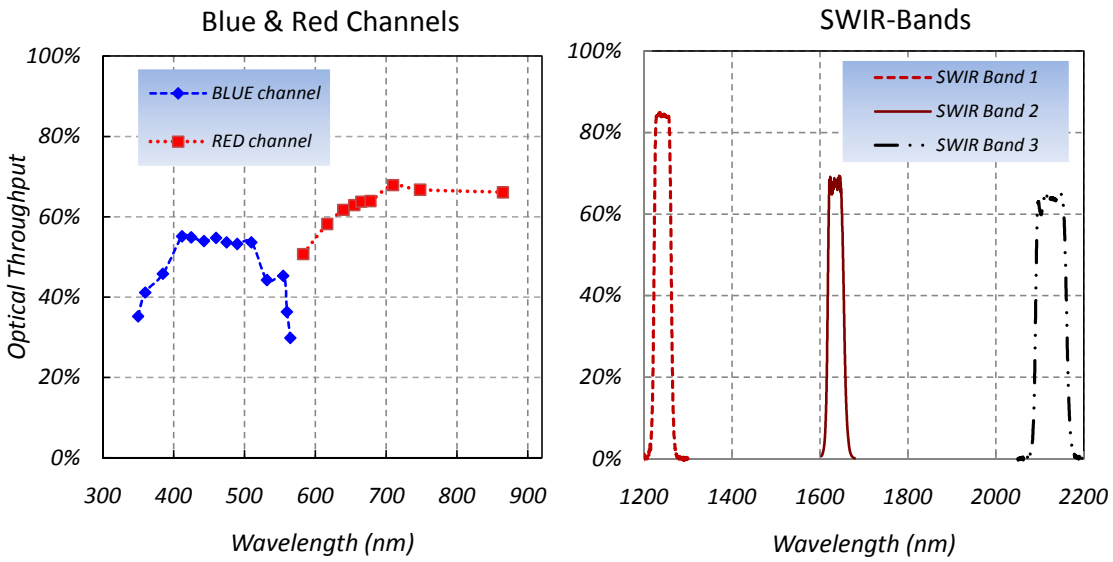

Figure 3.8: Total throughput for ORCA radiometer calculated from piece-part component data for blue and red channels (left) and three SWIR bands (right).

Chapter 4

System-Level Performance

We are now in a position to calculate the total system-level throughput from the piece-part data we have shown in previous sections. These results will provide a prediction of ORCA maximum throughput and they will form the basis to conclude whether ORCA will meet its radiometric sensitivity goals.

4.1 Throughput

The left panel of Fig. 3.8 illustrates the total efficiency response form the blue and red channels of ORCA. These curves are derived by multiplying the average spectral response of each of the components in the ORCA optical train, including the grating efficiencies. An analysis of these results when compared to typical surface-leaving radiance indicate that ORCA will meet or exceed the radiometric performance of either MODIS or SeaWiFS. These calculations show that ORCA should have not problem in meeting its sensitivity requirement goals in order to deliver ocean-color data product over the 20 aggregated bands in the 350-885 nm wavelength range. The overall efficiency is decidedly lower in the blue channel, when compared to the red-channel results. However, we should point out that measuring surface-leaving radiance in the red-channel spectral range will be more challenging given that signals there are much weaker. Hence, the higher sensitivity from these piece-part data would compensate for these weaker signals in the red band. The right panel Fig. 3.8 shows similar calculations done for the three bands in the three SWIR bands. These curves provide information about the total throughput as well as the spectral bandwidth for each of those bands. This is on account that narrow-band filters are used to define the transmission band-pass in each of the three SWIR bands. We will discuss next imaging performance for the blue and red channels. This discussion will be followed by a presentation of system-level spectral resolution results.

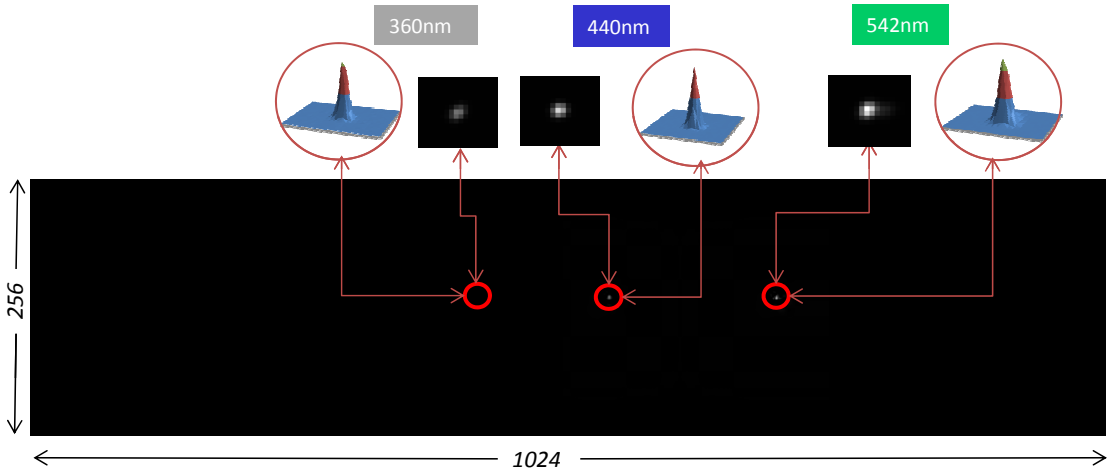

Figure 4.1: PSF images at three selected wavelengths in the blue-channel focal plane array.

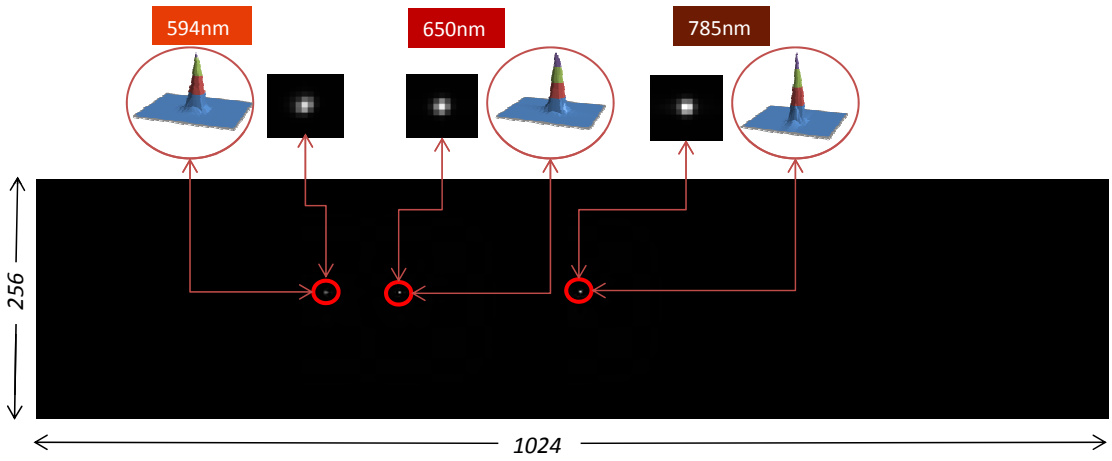

Figure 4.2: PSF images at three selected wavelengths in the red-channel focal plane array.

4.2 Point Spread Function

In addition to the spectral throughput discussed above, the imaging performance is a crucial element to ensure that ORCA will meet its science goals. This performance is strongly influenced by the wavefront error of the individual components that form the radiometer optical system. Measurements at the component-level wavefront error showed that they all met specification requirements. However, there is not enough space here to discuss these results in much detail. Instead, we have chosen to evaluate the overall imaging performance by studying the characteristics of the image or Point Spread Function (PSF) of a point source formed by ORCA at the instrument focal plane.

This point source consisted of a pinhole ($\simeq$ 200 μm) illuminated with several laser sources of known wavelengths. This pinhole was placed at best focus of a collimator consisting of an off-axis parabolic mirror. The output of this collimator was directed into the entrance aperture of ORCA. Recording of the image formed at the instrument focal plane was possible by installing non-flight commercial off-the-shelf (COTS) CCD array detectors on each of ORCA blue- and red-channel focal planes. The format for these arrays was 1024×256 pixels with individual pixel size of 26×26 μm^2. Although these arrays were oversized and they would not be able to handle data transfer rate in scanning mode, the physical pixel size was nearly identical to the proposed flight versions. Therefore, they were considered adequate for alignment and optical performance testing in static mode.

The results of these tests on the blue-channel focal plane are shown in Fig. 4.1, while red-channel PSF plots are shown in Fig. 4.2. These figures show a picture of the CCD full extent with simultaneous pinhole images of three laser wavelengths at 360, 440, and 543 nm for the blue channel. Similar results are shown for wavelengths at 594, 650, and 785 nm for the red channel. Further details are indicated by arrows pointing to magnification of the respective images at each of these wavelengths. Both figures also show arrows pointing to 3-D plots to illustrate the intensity profile for each of these pinhole images. Visual inspection indicates the image peaks are fairly sharp, whereas quantitative analyses show that more than 60% of the energy is concentrated within 1 to 2 physical pixels. The Airy diameter at visible wavelength is much smaller than a detector pixel size and therefore diffraction was not a driving consideration in the radiometer overall imaging performance. However, the requirement in the optical design was set so that spot size diagrams at any wavelength within the instrument spectral range, as well as any point along the full extend of the slit spatial dimension, to be less than two physical detector pixel sizes. Any curvature at the slit image plane and geometric aberrations were corrected through the design of a F/1.5 lens system used to focus the light at the detector image plane. We found that most of the aberration was in the spatial or along-track slit direction. Hence, this was not a cause for major concern, given that the energy is smeared in this direction as a result of the Time Delay Integration (TDI) for the instrument in scanning mode. The results shown in Figures 4.2 and 4.1 indicate that these goals were essentially met and we found the imaging performance of ORCA is a factor of three or better than that of the SeaWiFS radiometer.[2]

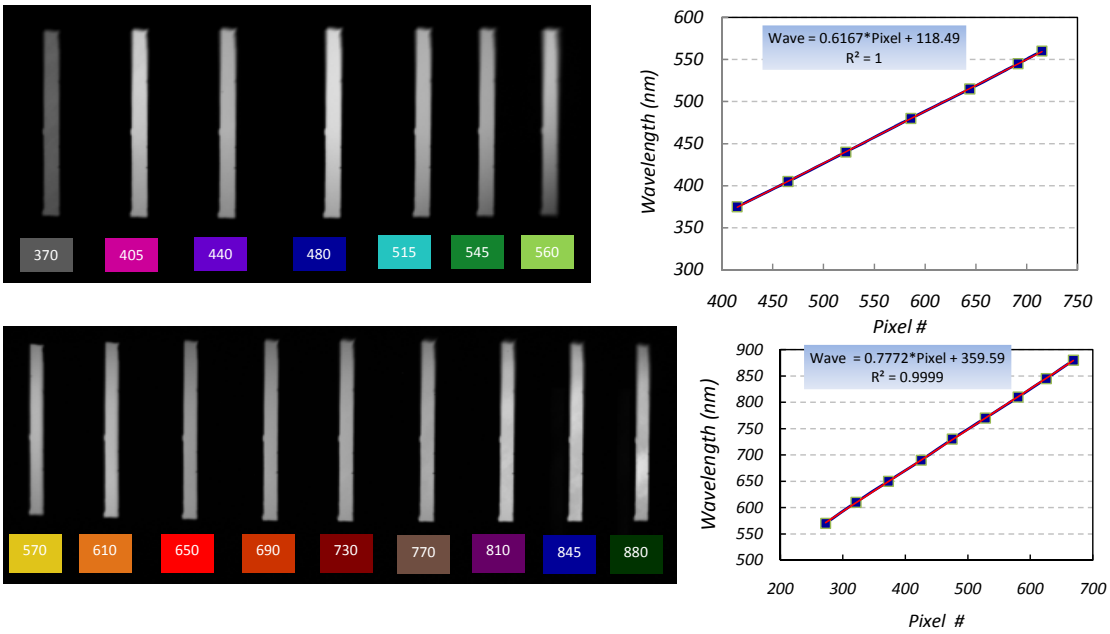

Figure 4.3: Left panel: Collection of slit images at various laser wavelengths for ORCA blue (top) and red (bottom) channels. Right panel: Linear plot of wavelength *vs* pixel location from the corresponding images on the left.

4.3 Dispersion

As mentioned previously, the ORCA optical design incorporates gratings in the blue and red channels to provide the proper wavelength separation. Because of how gratings are implemented in this design, it is not possible to get the overall system dispersion characteristics by just looking at the grating dispersion properties alone. The testing configuration consisted of placing ORCA in front of an integrating sphere that was coupled to a tunable laser that allowed the instrument to be illuminated with monochromatic light of known wavelength. The sphere had an output aperture size larger than that of ORCA in order to have the slit uniformly illuminated. A series of images were recorded at varying laser wavelengths. Performing these tests required relocating the instrument to one of the radiometric laboratories at the National Institute of Standards and Technology (NIST) using the Spectral Irradiance and Radiance Responsivity Calibrations Uniform Sources (SIRCUS).

The top-left panel of Figure 4.3 shows results of a series of images taken at various SIRCUS laser wavelengths in the corresponding spectral range for the blue channel. The bottom-left panel shows the same for the red channel. These figures show projections of the slit images on the CCD arrays of either channel. The extend along the vertical (spatial) direction is roughly 135 pixels and this corresponds to a 1 Km instantaneous field of view coverage on the ground. The horizontal dimension corresponds to the spectral direction. The extent and separation of the slit images along this direction provide information about the instrument dispersion properties. For instance, the FWHM along the spectral direction for the slit images shown in Fig. 4.3 are ~ 8 and ~ 8.5 pixels for the blue and red channels respectively. We also performed centroid determination along the spectral direction in each of these slit images on the CCD arrays and plotted these pixel locations *vs* their corresponding wavelengths in order to estimate the instrument dispersion and wavelength calibration performance. The right panels of Fig. 4.3 show the results of this analysis. In the case of the blue channel, the slope yields a value of 0.62 nm/pixel while this number is 0.78 nm/pixel for the red band. Given that the blue-channel slit image extent along the spectral dimension is ~ 8 pixels (the size of a superpixel in ORCA), we find the overall spectral resolution is $\simeq 4.93$ nm/superpixel for the instrument blue channel. Similar calculations done for the red channel yield a spectral resolution of $\simeq$ 6.6 nm/superpixel. A comparison of these numbers with the goal of a spectral resolution of 5 nm/superpixel for either channel suggests that the result is right on target for the instrument blue channel, whereas this number is slightly higher for the red-channel spectral resolution requirement of 5 nm/superpixel. The solution for meeting the red-channel spectral resolution requirement will consist in modifying the groove density or spacing.

Chapter 5

Summary

In conclusion, the results obtained from component-level optical testing have validated the robustness of the optical system design for ORCA. All the optical components used in the ORCA prototype have been made using existing technology and their excellent performance have brought ORCA closer to a flight configuration. The predicted optical throughput from piece-part data, the system-level spectral resolution, and polarization sensitivity results have shown ORCA is in a position to meet or exceed the radiometric requirements of the Decadal Survey Aerosol, Cloud, and Ecology (ACE), the Ocean Ecosystem (OES) radiometer and the Pre-ACE climate data continuity mission (PACE).

Bibliography

[1] Charles R. McClain, Gene C. Feldman, Stanford B. Hooker, "An overview of the SeaWIFS project andstrategies for producing a climate research quality global ocean bio-optical time series," *Deep-Sea Res. II* **51**, pp. 5–42, 2004.

[2] Mark E. Wilson, Charles McClain, Bryan Monosmith, Manuel Quijada, Eugene Waluschka, Patrick L. Thompsona, Steven Brown, "Optical design of the ocean radiometer for carbon assessment," in *Earth Observing Systems XVI*, *Proc. SPIE* **8153**, 2011.

[3] Eugene Waluschka, Mark Wilson, Manuel Quijada, Brendan McAndrew, Leibo Ding, "Orca depolarizer," in *Polarization Science and Remote Sensing V*, *Proc. SPIE* **8160**, 2011.

[4] Edward Collect, *Field Guide to Polarization*, SPIE Field Guide vol. **FG05**, SPIE Press, Bellingham, Washington, 2005.

[5] John G. Hagopian, Stephanie A. Getty, Manuel Quijada, June Tveekrem, Ron Shiri, Patrick Roman, James Butler, Georgi Georgiev, Jeff Livas, Cleophus Hunt, Alejandro Maldonado, "Multiwalled carbon nanotubes for stray light suppression in space flight instruments," *Proc. SPIE* **7761**, p. 77610F, 2010.

REPORT DOCUMENTATION PAGE

Form Approved
OMB No. 0704-0188

1. REPORT DATE *(DD-MM-YYYY)*	2. REPORT TYPE	3. DATES COVERED *(From - To)*
28-04-2012	Technical Memorandum	

4. TITLE AND SUBTITLE

Ocean Radiometer for Carbon Assessment (ORCA)

5a. CONTRACT NUMBER

5b. GRANT NUMBER

5c. PROGRAM ELEMENT NUMBER

6. AUTHOR(S)

Manuel Quijada, Mark Wilson, Timothy Madison, Peter Petrone, and Charles McClain

5d. PROJECT NUMBER

5e. TASK NUMBER

5f. WORK UNIT NUMBER

7. PERFORMING ORGANIZATION NAME(S) AND ADDRESS(ES)

National Aeronautics and Space Administration
Goddard Space Flight Center
Greenbelt, Maryland 20771

8. PERFORMING ORGANIZATION REPORT NUMBER

9. SPONSORING/MONITORING AGENCY NAME(S) AND ADDRESS(ES)

National Aeronautics and Space Administration
Washington, DC 20546-0001

10. SPONSORING/MONITOR'S ACRONYM(S)

NASA

11. SPONSORING/MONITORING REPORT NUMBER

NASA/TM–2012-215895

12. DISTRIBUTION/AVAILABILITY STATEMENT

Unclassified—*Available Only with Approval of Issuing Office (Ocean Ecology Laboratory)*, Subject Category: 35, 43, 48, Report available from GSFC—Ocean Ecology Laboratory, Code 616, Building 28 W107, Greenbelt, MD 20771. (301) 286-5377

13. SUPPLEMENTARY NOTES

14. ABSTRACT

A team at the Goddard Space Flight Center (GSFC) led by Principal Investigator Charles McClain (GSFC; Code 616) has been working on a functional ORCA prototype with flightlike fore and aft optics and scan mechanisms. As part of the development efforts to bring ORCA closer to a flight configuration, we have conducted component-level optical testing and system-level characterizations using non-flight commercial off-the-shelf (COTS) focal plane array detectors. The purpose of this paper is to describe the results of these testings performed at GSFC and the National Institute of Standards and Technology (NIST) at the component and system-level testings respectively.

15. SUBJECT TERMS

Earth resources, remote sensing, ocean color, oceanography, biological oceanography, chlorophyll concentration, marine biology, phytoplankton concentration, instrumentation, instrument design, radiometers, Earth sensors, sensor performance

16. SECURITY CLASSIFICATION OF:			17. LIMITATION OF ABSTRACT	18. NUMBER OF PAGES	19b. NAME OF RESPONSIBLE PERSON
a. REPORT	b. ABSTRACT	c. THIS PAGE			Charles McClain
Unclassified	Unclassified	Unclassified	Unclassified	43	19b. TELEPHONE NUMBER *(Include area code)* (301) 286-5377